Electrokinetic Molecular Separation in Nanoscale Fluidic Channels

ARTICLE *in* LAB ON A CHIP · NOVEMBER 2005

Impact Factor: 6.12 · DOI: 10.1039/b503914b · Source: PubMed

8 AUTHORS, INCLUDING:

Linnea K Ista
University of New Mexico
51 PUBLICATIONS **1,769** CITATIONS
SEE PROFILE

Dimiter Petsev
University of New Mexico
96 PUBLICATIONS **2,723** CITATIONS
SEE PROFILE

Andrea alberto Mammoli
University of New Mexico
72 PUBLICATIONS **998** CITATIONS
SEE PROFILE

Steven Brueck
University of New Mexico
453 PUBLICATIONS **8,179** CITATIONS
SEE PROFILE

Electrokinetic molecular separation in nanoscale fluidic channels

Anthony L. Garcia,[a] Linnea K. Ista,[b] Dimiter N. Petsev,[b] Michael J. O'Brien,[b] Paul Bisong,[b] Andrea A. Mammoli,[a] Steven R. J. Brueck[c] and Gabriel P. López*[b]

Received 17th March 2005, Accepted 22nd August 2005
First published as an Advance Article on the web 12th September 2005
DOI: 10.1039/b503914b

This report presents a study of electrokinetic transport in a series of integrated macro- to nano-fluidic chips that allow for controlled injection of molecular mixtures into high-density arrays of nanochannels. The high-aspect-ratio nanochannels were fabricated on a Si wafer using interferometric lithography and standard semiconductor industry processes, and are capped with a transparent Pyrex cover slip to allow for experimental observations. Confocal laser scanning microscopy was used to examine the electrokinetic transport of a negatively charged dye (Alexa 488) and a neutral dye (rhodamine B) within nanochannels that varied in width from 35 to 200 nm with electric field strengths equal to or below 2000 V m^{-1}. In the negatively charged channels, nanoconfinement and interactions between the respective solutes and channel walls give rise to higher electroosmotic velocities for the negatively charged dye than for the neutral dye, towards the negative electrode, resulting in an anomalous separation that occurs over a relatively short distance (<1 mm). Increasing the channel widths leads to a switch in the electroosmotic transport behavior observed in microscale channels, where neutral molecules move faster because the negatively charged molecules are slowed by the electrophoretic drag. Thus a clear distinction between ''nano-'' and ''microfluidic'' regimes is established. We present an analytical model that accounts for the electrokinetic transport and adsorption (of the neutral dye) at the channel walls, and is in good agreement with the experimental data. The observed effects have potential for use in new nano-separation technologies.

Introduction

Elucidation of phenomena associated with the flow of liquids through conduits of nanoscale dimensions remains an important scientific goal as nanofluidic devices receive increased attention. Specifically, the development of chip-based nanofluidic systems for molecular (especially biomolecular) separations based on nanoscale phenomena including entropic trapping[1] and shear-driven chromatography[2] has recently received intense interest. In addition to a limited number of experimental efforts[3–8] several important theoretical studies have sought to clarify the effects of nanoconfinement of fluids on the transport of ions and molecules in electrokinetic flows.[9–11] For example, a recent study by Qiao and Aluru concluded that effects resulting from the non-continuum nature of electrokinetic flows in nanoscopic pores are associated with varying fluid viscosity very close to the pore wall.[12] Further, with this correction, electroosmotic velocity profiles more than a few molecular layers away from solid surfaces are in reasonable accordance with the continuum theory.[13,14]

The goals of this study are (i) to develop methodologies for investigation of electrokinetic transport in nanoscale channels (averaged across many nanochannels) using confocal scanning laser microscopy, a widely available far-field technique, and (ii) to explore the potential use of nanoconfined electrokinetic transport in molecular separations. For the purpose of this study, we use the term nanoconfinement to refer to a situation in which electrical double layers that form in the presence of charged channel walls (Debye screening layers) extend into the channel significantly, thus representing a significant percentage of the channel width, and thereby effecting the nature of the electroosmotic velocity profiles. For solutions with ion concentrations relevant to separation of biomolecules, this leads to more complex electroosmotic velocity profiles than the usual ''plug-like'' flow observed in capillaries of larger sizes.[14]

Charged solutes in electrolyte solutions that are electrokinetically driven through channels with nanoscale widths exhibit unique transport characteristics that may provide significant technological benefits because most biomolecules (DNA, proteins, peptides) are charged, or can be complexed with charged surfactant molecules. The significant alteration of the velocities of these species in electrokinetic and pressure-driven flows through channels of nanoscopic widths may enable efficient separations over short lengths not possible in channels of macroscopic or even microscopic width.

Chip fabrication

We used silicon-based T-chips, integrating an array of parallel nanochannels with microchannels for fluid control and macroscopic injection ports, to study the electrokinetic transport of fluorescent dyes in nanochannels (Fig. 1A).[15] The different T-chips incorporate nanochannels that range

[a]*Department of Mechanical Engineering, Albuquerque, New Mexico 87131*
[b]*Dept. of Chemical and Nuclear Engineering and Dept. of Chemistry, Albuquerque, New Mexico 87131. E-mail: gplopez@unm.edu*
[c]*Center for High Technology Materials and Dept. of Electrical and Computer Engineering, University of New Mexico, Albuquerque, New Mexico 87131*

from 35 to 200 nm in width in the plane of the chip, while being deep enough to allow significant molecular throughput and to provide large enough signals for facile detection by laser-induced fluorescence microscopy. The high aspect ratio of the channels is amenable to description by relatively simple analytical models that allow interpretation of the results of our experimental system. Other advantages, as well as fabrication details have been discussed elsewhere.[15] The nanochannel section (1 mm in width and consisting of $\sim$2000 parallel nanochannels) is located within Arm 3 of the T-Chip (Fig. 1A), and originates at the intersection of the microchannels and extends 1 cm down Arm 3. A cross-sectional scanning electron micrograph of a small number of nanochannels in one of the T-chips used for this study is shown in Fig. 1B. In this chip, the channels are approximately 50 nm wide by 500 nm deep, and are on a 400 nm pitch. The channel width is sufficiently narrow to result in interaction between the diffuse double layers extending from opposite sides of the channel walls. Fluorescence from the dye molecules in the fluid is monitored through the transparent lid using confocal microscopy. While the details for the flow profiles in the individual nanochannels are below the resolution limit of conventional optical microscopy, average velocities of dye fronts can be monitored and provide insight into the electrokinetic transport mechanisms in the nanochannels.

Experimental results

Electrokinetic separations used a buffer containing 0.25 mM tris-(hydroxy)aminomethane hydrochloride and 1.92 mM glycine at pH 8.8 (*viz*., a 1/100 dilution of the standard poly(acrylamide) gel electrophoresis buffer). The ionic strength of this buffer was estimated to be $\sim$0.35 mM as calculated from the pK_as of each salt. At this ionic strength we estimate the magnitude of the Debye screening length ($1/\kappa$, see below) to be $\sim$16 nm. The buffer was filtered through a 0.2 μm filter to remove particulate contaminants and then degassed under vacuum for at least 3 h. Solutions of dyes (rhodamine B (MW = 479 Da) and Alexa 488 maleimide (MW = 720 Da), Molecular Probes Inc.) were prepared in this buffer, each at a concentration of 5 mg mL^{-1}. At pH 8.3, rhodamine B is neutral and Alexa 488 maleimide has a charge of -2.[16] The addition of Alexa contributes a negligible increase in the ionic strength of the bulk solution.

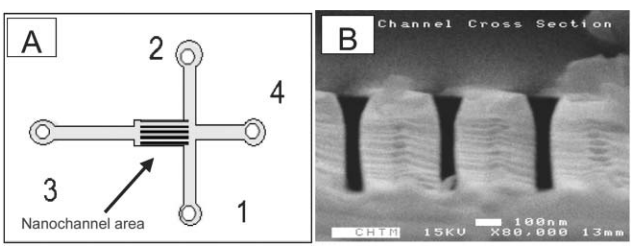

Fig. 1 (A) Top view (schematic) of the integrated chips. The holes are numbered for reference, and nanochannel area is noted. The channels are 3 cm long from well 3 to well 4, and 2 cm from well 1 to well 2. (B) SEM image of the cross section of the nanochannel array (50 nm wide nanochannels) in a chip taken after experiments were performed showing a Pyrex lid bonded to the oxidized silicon trenches to form channels.

Electrode 2 (see Fig. 1A) was grounded, while the remaining three electrodes were attached to the outputs of three separate DC power supplies. The chip was filled with buffer (no dyes) *via* capillary action from well 3 and placed under an upright, laser-scanning confocal microscope (Zeiss Axioskop with an LSM5 scanning head). Ten μL of a 1 : 1 mixture of the two dye solutions were introduced into well 1, and initially Electrode 1 was set to +30 V relative to Electrode 2 (Electrodes 3 and 4 were set to 0 V) so that the solution moved from well 1 towards well 2 by electroosmosis in the microchannel. Separation of the two dyes was not observed in the microchannels during this step. Once the dye mixture (as monitored by fluorescence microscopy) reached the T-intersection, Electrode 1 was set to 0 V and Electrode 4 was set to +30 V so the fluid flowed towards well 3 through the nanochannels *via* electroosmosis. Dye velocities were obtained by tracking the time evolution of the dye fronts through the nanochannel array.[17] At least thirty measurements of dye front velocities, throughout the cross section of the nanochannel arrays, were averaged to obtain the velocity corresponding to a given field strength.

Fig. 2 presents laser-induced fluorescence micrographs that demonstrate differential transport of the two dyes in channels with widths of $\sim$50 nm (left) and $\sim$200 nm (right). Dye fronts in the array of 200 nm-wide channels are observed to be more uniform. The smaller channels are more of a fabrication challenge and likely have larger percentage in width deviation leading to the observed variations in dye front uniformity. We performed a study to characterize the uniformity of the channels in which several SEM cross sections of the nanochannel arrays were taken at different places in the array. We measured the inhomogeneity of the channels to be approximately 4–6% deviation in 50 nm channels and a much smaller percentage deviation in wider channels. This inhomogeneity in the channel widths should not effect the data we collect because our measurements at low magnification average over quite a few channels ($\sim$100), which are spaced by less than the optical wavelength. Also the dye velocities for each chip and EO voltage were measured at different locations within the nanochannel array, and were not observed to differ greatly from region to region.

Separation of the dye fronts begins very close to the entry to the nanochannels (in all cases less than 1 mm from the entrance); the negatively charged dye (Alexa 488) had a faster velocity than the neutral dye (rhodamine B) towards the negatively biased electrode. This behavior is opposite to what is expected[14] for electrokinetic transport of the dyes in larger scale channels where electrophoresis toward the positive electrode slows the electroosmotic transport of the negatively charged species relative to the neutral one. By creating bands of dye, we were able to completely separate the two dyes within the nanochannel array. An example of this separation in 50 nm wide channels can be seen in Fig. 2E and 2F. Here a band of Alexa dye has exited the nanochannel array and is solely in the microchannel portion of arm 3 (Fig. 2F), while at the same time the rhodamine B dye has yet to reach this end of the nanochannels (Fig. 2E). In Fig. 2G and 2H we present another example of complete dye separation, (in channels $\sim$100 nm in

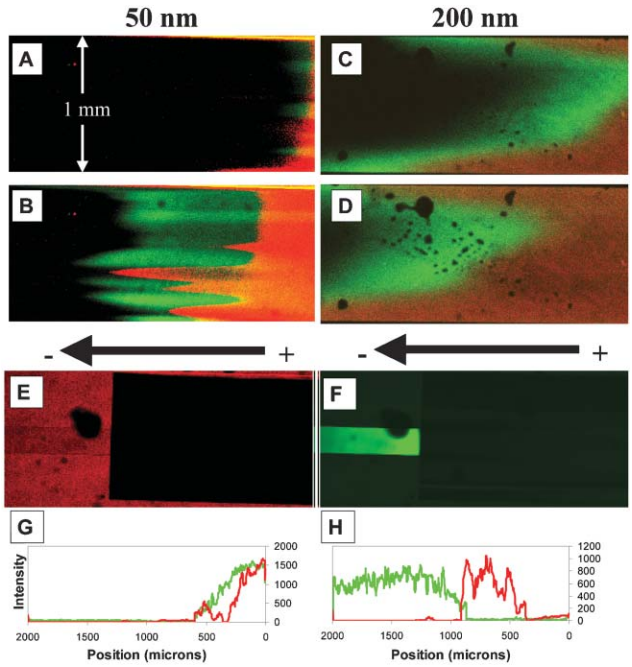

Fig. 2 Sample two-color fluorescence micrographs (green = Alexa 488, red = rhodamine B) showing separation of dyes in nanochannel arrays containing channels ~50 nm wide at (A) time $t = 0$ and (B) $t = 30$ s, and ~200 nm wide channels at (C) time $t = 0$ and (D) $t = 25.2$ s. (E) and (F) are micrographs of the far end of the nanochannel array near well 3 in which the red detector channel (E) and green detector channel (F) are shown separately. In the 50 nm channels at $t = 600$ s the green Alexa dye has exited the nanochannels completely and is solely in the microchannel (F) while the red rhodamine B dye has not reached the far end yet (E). (G) and (H) show fluorescence intensity profiles for the two dyes in ~100 nm wide channels at (G) time $t = 0$ s and (H) $t = 290$ s. The dark splotches in the micrographs are due to defects in the Pyrex lid formed during anodic bonding. They do not affect flow in the nanochannels.

width) that takes place within less than 2 mm from the nanochannel inlet, and within a few minutes. Fig. 2G shows bands in the fluorescence intensity profiles of the two dyes overlapping at the entrance of the nanochannel array at time $t = 0$, while Fig. 2H shows that a band of the negatively charged Alexa dye has moved further along the length of the array than a band of the neutral rhodamine B dye at a time $t = 290$ s. This separation was achieved with a relatively low electroosmotic voltage of 15 V.

We performed control experiments with a commercial micro T-Chip (50 μm-wide channel, Micralyne Inc.) and observed that the negatively charged Alexa lags behind rhodamine B. The commercial chip was selected because the surface of its walls is SiO_2, which is the same as the T-chip. The data that we have found in literature[18,19] as well as our own experimental measurements show that both chips have similar surface potentials. The isoelectric point of both chips is at a pH of roughly 2.6, and the surface charges change similarly with variations in buffer pH.

We observed the effects of electrical double layer overlap by changing the width of the nanochannels (~35, ~50, ~90, ~160, and ~200 nm wide) within test chips, while keeping the ionic strength constant. It is possible to achieve a qualitatively

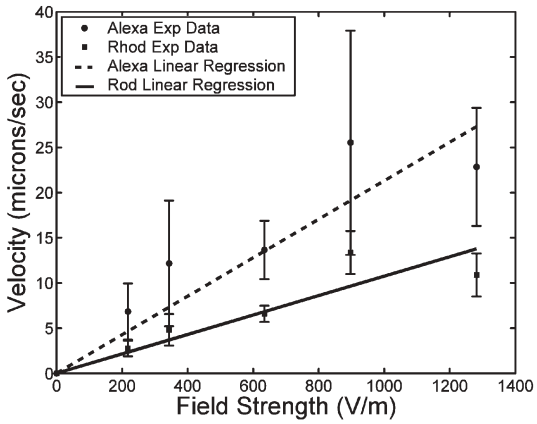

Fig. 3 Plot of the experimentally observed dye front velocity *vs.* field strength for both Alexa 488 and rhodamine B in 160 nm nanochannels. Error bars denote the standard deviation of the measured velocity.

similar objective by changing the ionic strength of the buffer at a constant channel width, however, the range of ionic strength of the buffer is limited due to practical restrictions. Field strengths used in our experiments ranged from 0 to 2000 V m^{-1}. Fig. 3 presents a representative data set collected for the chips with nanochannels 160 nm in width. In all cases a linear relationship (within experimental accuracy) was observed between the imposed electric field and the measured velocity of the dye front. Thus, for a single channel width, the ratios of the velocities of the two dyes are independent of the imposed electric field, which is as expected.[14] The variation in the reproducibility of the velocities of the two different dyes is due mainly to the low volumes of the dyes within the nanochannel array and our ability to precisely detect the dye fronts, however, the measured ratio of the dye velocities remains highly reproducible. As the width of the channel decreased from 200 nm to 35 nm, the ratio of the velocities of the dyes (v_{Alexa}/v_{rhod}) increased from 1.5 : 1 to 5.8 : 1 (see Fig. 4).

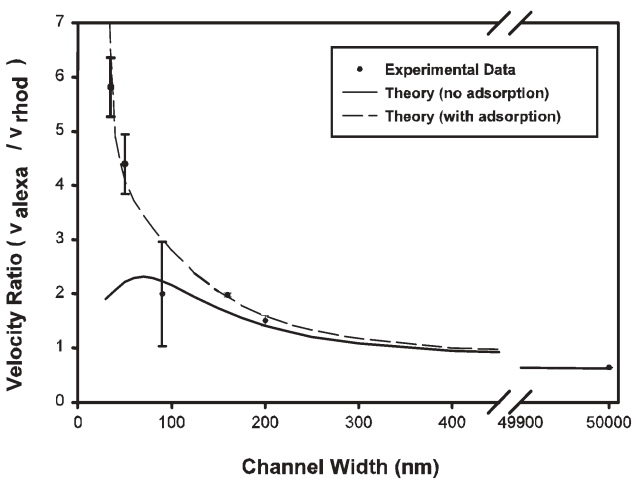

Fig. 4 Experimental and theoretical ratios of velocities of dyes (v_{Alexa}/v_{rhod}) *vs.* width of nanochannel. The experimental ratio is the ratio of the slopes of lines obtained by least squares linear regression of dye front velocity *versus* applied voltage. The theoretical ratios are obtained from eqn (5). Error bars are typically obtained by evaluating the standard deviation for velocities obtained at five different field strengths.

We considered two possible mechanisms for electrokinetic separations that occur in nanoscale channels, which are not observed in channels of larger dimensions (microchannels). The first is related to the segregation of the negatively charged Alexa dye toward the center of the nanochannels (away from the negatively charged walls) where the electroosmotic velocity is higher. The second is related to the adsorption of the neutral dye to the nanochannel walls. In the discussion below, we present a model that allows estimation of the relative contributions of these two mechanisms to the observed dye transport characteristics.

Theory

At sufficiently small scales, important dimensions such as the Debye screening length ($1/\kappa$)[20] and channel width d are of the same order. In the experiments described here, the product κd varied from $\sim$2 to 12. Described here is an approximation that allows for a theoretical treatment of the electrokinetic transport in these situations assuming a 2D flow field in channels with parallel walls and weak double layer overlap. Under these conditions, one may assume that the total electric potential between the walls of the nanochannels is simply the sum of the potentials of single walls.[14,21] With these assumptions, the dimensionless potential distribution across the width of an individual nanochannel is:[14]

$$\Psi(x) = \frac{4kT}{ze}\left[\tanh^{-1}\left(\tanh\left[\frac{ze\zeta}{4kT}\right]\exp(-\kappa x)\right)\right] + \frac{4kT}{ze}\left[\tanh^{-1}\left(\tanh\left[\frac{ze\zeta}{4kT}\right]\exp(-\kappa(d-x))\right)\right] \quad (1)$$

Here z is the valency of the background electrolyte, ζ is the electrokinetic (zeta) potential of the nanochannel walls, $\kappa = [(2e^2z^2C_{el})/(kT\varepsilon_0\varepsilon)]^{1/2}$, e is the electronic charge, C_{el} is the electrolyte's number concentration, ε_0 is the dielectric permittivity of free space, ε is the relative dielectric constant of the solvent, and kT is the thermal energy. This approximation is valid for an arbitrarily high surface potential and $\kappa d \geqslant 2$.[20] Since the double layers from the channel walls occupy a substantial portion of the channel, the resulting electroosmotic velocity profile ($v_{eo}(x)$) is not 'plug-like' (as it is in wider microchannels), but follows the shape of the potential ($\psi(x)$). Hence, the closer to the channel center, the faster the fluid flow. The electroosmotic and average electroosmotic velocity across a channel are given by:[14]

$$v_{eo}(x) = -\frac{\varepsilon\varepsilon_o\zeta E}{d\eta}\left[1-\frac{\Psi(x)}{\zeta}\right],\ \bar{v}_{eo} = \frac{1}{d}\int_0^d v_{eo}(x)\mathrm{d}x \quad (2)$$

where η is the solvent viscosity. The concentration distribution of a solute across the nanochannel and the average concentration are:

$$C(x) = C_o\exp\left[-\frac{z_A e\Psi(x)}{kT}\right],\ \bar{C} = \frac{1}{d}\int_0^d C(x)\mathrm{d}x \quad (3)$$

where C_0 is the solute concentration in the microchannel feeding the nanochannel array and z_A is the charge of the solute.

Separation of the two dyes within nanochannels can occur because the negatively charged walls repel the negatively charged dye which is forced to the center of the channel (eqn (3)). Thus, a significant portion of the charged dye occupies the region of fluid that moves fastest towards the negative electrode. The total convective flux is, by definition, concentration $\times$ fluid velocity. Since, for the negatively charged dye, both concentration and velocity have a maximum at the channel center, the effective flux of the negatively charged dye peaks sharply near the channel center. Eqn (4) describes the concentration-weighted velocity of a dye within a nanochannel.

$$v(x) = \frac{C(x)v_{eo}(x)}{\bar{C}} - v_{ep} \quad (4)$$

Here v_{ep} is the electrophoretic velocity of the negatively charged dye.

In contrast, the neutral dye is not repelled from the walls by the long-range electrostatic force, rather it distributes uniformly across the channel, and its concentration profile does not have a maximum at the center, although the fluid velocity still does. Thus, averaged across the nanochannel, it exhibits a slower velocity. In addition, molecular adsorption to the channel walls, can significantly affect separations in nanoscale channels. The charged Alexa dye is electrostatically repulsed from the nanochannel walls, preventing it from adsorbing, however, a portion of the neutral rhodamine B molecule does adsorb,[22] diverting part of its flux in a direction toward the channel walls. This leads to an additional apparent "drag" for the neutral dye, reducing its net forward flux, and resulting in an overall slower velocity. For the channel geometries investigated, the wall area available for adsorption remains approximately constant as the channel width decreases; however, the total number of dye molecules in the channel decreases with the volume of the channel. Thus, the adsorption effect becomes much more significant with decreasing channel width (*i.e.*, increasing channel surface to volume ratio).

Since rhodamine B is neutral, it is transported through the nanochannel array only by electroosmosis. Thus, by measuring the velocity in wider channels (*e.g.* microchannels) where we can assume that the drag due to adsorption is negligible, we can use eqn (2) to obtain the zeta potential, ζ. Using the velocity of rhodamine B for the 200 nm channels, we estimated ζ = 81 mV, which is comparable to zeta potentials in oxidized silicon chips reported elsewhere.[23] This value of ζ was used in the equations above to estimate the dye velocities for all other nanochannel sizes (see below).

Fig. 5 shows the normalized species velocity profiles (due to electroosmosis) of the two dyes derived from eqn (4) for 200 nm and 60 nm-wide nanochannels neglecting electrophoresis. Eqn (4) predicts that the greatest difference in the maximum electrokinetic velocities will be observed at approximately 60 nm (see Fig. 4); below this width ($\kappa d \sim 4$) the extent of double layer overlap reduces the potential variation across the channel, and hence the development of electroosmotic velocity profiles.

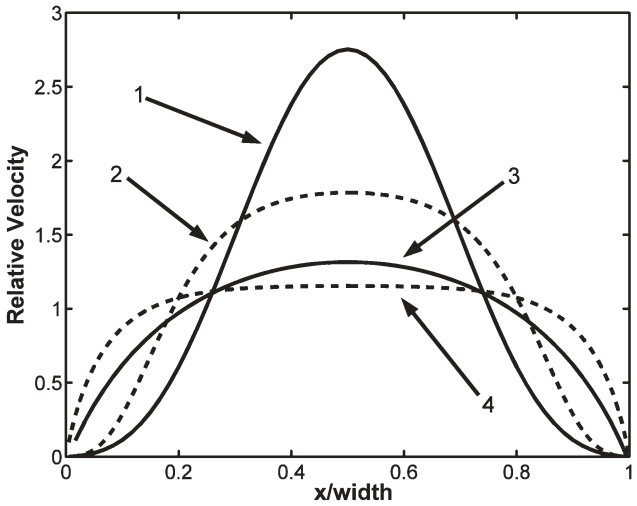

Fig. 5 Dimensionless species velocity profiles $c(x)v_{eo}$ $(x)/\bar{c}\bar{v}_{eo}$ due to electroosmosis for the negatively charged dye (Alexa 488) in (1) 60 nm and (2) 200 nm-wide channels and for the uncharged dye (rhodamine B) in (3) 60 nm and (4) 200 nm channels.

Taking into account electroosmosis, electrophoresis, and adsorption, the ratio of the maximum dye velocities may be represented by eqn (5).

$$\frac{v_{\text{charged}}}{v_{\text{neutral}}} = \frac{j_{\text{charged}} - j_{\text{electrophoresis}}}{j_{\text{neutral}} - \left(c_{\text{adsorption}}/d\right)} \quad (5)$$

Here j_{charged} and j_{neutral} are the calculated maximum electroosmotic fluxes of the charged (Alexa 488) and neutral (rhodamine B) dyes, respectively, and $c_{\text{adsorption}}$ is the kinetic adsorption coefficient which was obtained by fitting to the data for all nanochannel widths. The value of this coefficient is $\sim$23 moles/(nm s^{-1}). The adsorption flux scales inversely with the surface to volume ratio ($1/d$). The electrophoretic flux, $j_{\text{electrophoresis}}$, was measured for Alexa 488 in a microchannel of known width (50 μm).[24]

A plot of the theoretical ratio of velocities with and without adsorption, from eqn (5), along with the experimentally measured ratios, as a function of nanochannel width, is given in Fig. 4. Using this plot we estimate that below a width of $\sim$400 nm ($\kappa d \sim 25$), the flux of the negatively charged species towards the negatively charged electrode is greater than the flux of the neutral species. Also based on Fig. 4, one can see that the dominant mechanism for separation of these dyes in channels ranging from $\sim$60 to 400 nm in width is the electrostatic segregation of the negatively charged dye towards the center of the channel where electroosmotic flux is maximum. Adsorption of the neutral dye plays a more significant role in separations in channels below $\sim$60 nm in width (based on the differences between the curve that accounts for adsorption and the curve without adsorption and the horizontal line where the velocity ratio is equal to one). There is good agreement between the model and our experimental observations for channel widths ranging from 35 nm to 50 μm. Similar separation of the dyes, resulting from parabolic velocity profiles, was also achieved by applying a pressure gradient to drive the fluid in the channels (data not shown).

Conclusion

In conclusion, we have shown that nanoconfinement of electrokinetic transport results in well-behaved separation of dyes, which differs from that typical of larger fluidic systems and, importantly, which can be observed at much shorter distances. Spatially averaged electrokinetic transport in these nanoscale channels can effectively be observed by confocal scanning laser fluorescence microscopy. The experimental data agrees well with a continuum-based analytical model for which the ratio of dye velocities increases as channel width decreases, because of increased localization of the charged dye in the center of the channel, where the electroosmotic flow velocity is greatest, and because of adsorption of the neutral dye on the channel walls. Under the ionic strength conditions of this study, the electrokinetic model is expected to remain valid in channels wider than $\sim$30 nm ($\kappa d \sim 2$), below which, the assumption of weak double layer overlap breaks down. Further refinement of the model will take into account the shape of the channel cross section. We have begun to quantify the effectiveness of pressure driven separations of these solutes, and to investigate other molecular species including peptides, proteins and DNA. Decreasing the nanochannel width leads to qualitatively new and counterintuitive behavior that can be exploited for molecular separations.

Acknowledgements

We thank Dr K. Artyushkova and Mr R. Bradley for technical assistance, and Dr S. Sibbett for critical reading of this manuscript. Funding for this work was provided by the NSF (NER: CTS-0304237, NIRT: CTS-0404124 IGERT: DGE-00114319) and the W. M. Keck Foundation. Additional funding for personnel salaries was provided by the ARO and the Intel Corporation. Images in this paper were generated at the University of New Mexico Cancer Research Facility.

References

1 J. Han, S. W. Turner and H. G. Craighead, *Phys. Rev. Lett.*, 1999, **86**, 1394.
2 D. Clicq, N. Vervoort, R. Vounckx, H. Ottevaere, J. Buijs, C. Gooijer, F. Ariese, G. V. Baron and G. Desmet, *J. Chromatogr.*, 2002, **979**, 33.
3 S. C. Jacobson, J. P. Alarie and J. M. Ramsey, in *Proceedings of Micro Total Analysis Systems*, Dordrecht, The Netherlands, 2001, 57–59.
4 R. Karlsson, M. Karlsson, A. Karlsson, A. S. Cans, J. Bergenholtz, B. Akerman, A. G. Ewing, M. Voinova and O. Orwar, *Langmuir*, 2002, **18**, 4186.
5 D. Stein, M. Kruithof and C. Dekker, *Phys. Rev. Lett.*, 2004, **93**, 035901.
6 J. T. Cheng and N. Giordano, *Phys. Rev. E*, 2002, **65**, 031206.
7 P. J. Kemery, J. K. Steehler and P. W. Bohn, *Langmuir*, 1998, **14**, 2884.
8 Q. S. Pu, J. S. Yun, H. Temkin and S. R. Liu, *Nano Lett.*, 2004, **4**, 1099.
9 A. P. Thompson, *J. Chem. Phys.*, 2003, **119**, 7503.
10 K. P. Travis and K. E. Gubbins, *J. Chem. Phys.*, 2000, **112**, 1984.
11 H. Daiguji, P. D. Yang, A. J. Szeri and A. Majumdar, *Nano Lett.*, 2004, **4**, 137.
12 R. Qiao and N. R. Aluru, *J. Chem. Phys.*, 2003, **118**, 4692.
13 C. L. Rice and R. J. Whitehead, *Phys. Chem.*, 1965, **69**, 4017.
14 R. J. Hunter, *Zeta Potential in Colloid Science: Principles and Applications*. Academic Press: London, 1981.

15 M. J. O'Brien, P. Bisong, L. K. Ista, E. M. Rabinovich, A. L. Garcia, S. S. Sibbett, G. P. Lopez and S. J. Brueck, *J. Vac. Sci. Technol. B*, 2003, **21**, 2941.
16 http://www.probes.com/.
17 D. Sinton and D. Li, *Colloids Surf., A*, 2003, **222**, 273.
18 P. J. Scales, F. Greiser, T. W. Healy, L. R. White and D. Y. C. Chan, *Langmuir*, 1992, **8**, 965.
19 D. J. Riley and R. G. Carbonell, *J. Colliod Interface Sci.*, 1993, **158**, 259.
20 W. B. Russel, D. A. Saville and W. R. Schowalter, *Colloidal Dispersions*, Cambridge University Press, 1989.
21 E. J. Verwey and J. T. Overbeek, *Theory and Stability of Lyophobic Colloids*. Elsevier: Amsterdam, 1948.
22 G. Drazer, *Phys Rev Lett.*, 2002, **89**, 244501.
23 B. J. Kirby and E. F. Hasselbrink, *Electrophoresis*, 2004, **25**, 187.
24 We also fit the data using a model with only adsorption driving the separation, using two fitting parameters representing the kinetic adsorption coefficients for each dye. This resulted in a negative adsorption coefficient for the negatively charged Alexa dye, meaning this dye exhibits negative adsorption (*i.e.* repulsion which our model shows is likely due to Debye-layer effects).